



pubs.acs.org/JACS Article

Atomic Resolution Insights into pH Shift Induced Deprotonation Events in LS-Shaped A β (1–42) Amyloid Fibrils

Nina Becker, Benedikt Frieg, Lothar Gremer, Tatsiana Kupreichyk, Luis Gardon, Patrick Freiburg, Philipp Neudecker, Dieter Willbold, Holger Gohlke,* and Henrike Heise*



Cite This: J. Am. Chem. Soc. 2023, 145, 2161–2169



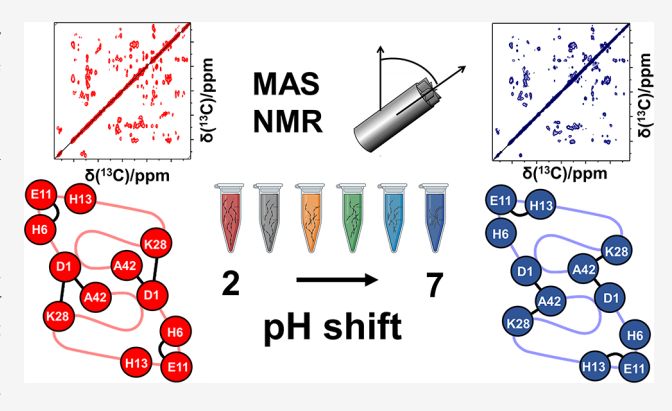
ACCESS I

Metrics & More

Article Recommendations

sı Supporting Information

ABSTRACT: Alzheimer's disease is a neurodegenerative disorder associated with the deposition of misfolded aggregates of the amyloid- β protein (A β). A β (1–42) is one of the most aggregation-prone components in senile plaques of AD patients. We demonstrated that relatively homogeneous A β (1–42) fibrils with one predominant fold visible in solid-state NMR spectra can be obtained at acidic pH. The structure of these fibrils differs remarkably from some other polymorphs obtained at neutral pH. In particular, the entire N-terminal region is part of the rigid fibril core. Here, we investigate the effects of a pH shift on the stability and the fold of these fibrils at higher pH values. Fibril bundling at neutral pH values renders cryo-EM studies impractical, but solid-state NMR spectroscopy, molecular dynamics simulations, and biophysical methods provide residue-specific structural information



under these conditions. The LS-fold of the $A\beta(1-42)$ fibrils does not change over the complete pH range from pH 2 to pH 7; in particular, the N-terminus remains part of the fibril core. We observe changes in the protonation state of charged residues starting from pH 5 on a residue-specific level. The deprotonation of the C-terminal carboxyl group of A42 in the intermolecular salt bridge with D1 and K28 is slow on the NMR time scale, with a local p K_a of 5.4, and local conformations of the involved residues are affected by deprotonation of A42. Thus, we demonstrate that this fibril form is stable at physiological pH values.

■ INTRODUCTION

The deposition of amyloid plaques consisting of amyloid β peptide $(A\beta)$ is one of the pathological hallmarks of Alzheimer's disease (AD). The predominant species of $A\beta$ in the brain are peptides containing 39 to 43 amino acid residues generated from the cleavage of amyloid precursor protein (APP) by β - and γ -secretases. The two prevalent forms are $A\beta(1-40)$ and $A\beta(1-42)$. The latter is more toxic and shows a higher aggregation propensity. The latter is more toxic and shows a higher aggregation propensity.

In recent years, several 3D structures of $A\beta(1-42)$ fibrils were solved using solid-state nuclear magnetic resonance (NMR) spectroscopy and cryogenic electron microscopy (cryo-EM).^{5–8} In a recent study on brain-derived $A\beta(1-42)$ fibrils from brains of 10 individuals with different $A\beta$ -associated neurodegenerative diseases (among them sporadic and familial Alzheimer's disease), two different structures were solved using cryo-EM. Interestingly, both fibril types seem to coexist in most AD-related brain tissues, although with different propensities.⁹ Likewise, recent solid-state NMR investigations of $A\beta(1-42)$ fibrils showed that $A\beta(1-42)$ fibrils seeded from brain material were polymorphic with distributions of polymorphs differing between nondemented older people and Alzheimer's disease patients.¹¹ Polymorphism

for brain-seeded A $\beta(1-42)$ fibrils was also observed by Ishii and co-workers by ¹H detected solid-state NMR spectroscopy, together with a novel fibril type for recombinantly expressed in vitro A β (1–42). Although the 3D fibril structures 5–9 could show that the fibrils consist of two intertwined protofilaments with the C-terminus describing an S-shaped conformation, substantial structural differences exist. Some structural differences may result from the preparation conditions, differing especially in pH values. For most A β fibrils grown at neutral pH values (pH 7.4-8), the N-terminus is disordered and not part of the fibril core, an exception being fibrils of the $A\beta(1-40)$ peptide with the Osaka mutation (E22 Δ). In most cases, for the generation of homogeneous $A\beta(1-42)$ fibril preparations repeated seeding was necessary.⁵⁻⁷ In vitro fibrillization of $A\beta(1-42)$ at an acidic pH value of 2 and in the presence of 30% acetonitrile, however, resulted in extremely

Received: August 30, 2022 Published: January 18, 2023





slow fibril growth over several weeks. In the resulting fibril preparations, fibrils are well separated from each other, as the acetonitrile prevents formation of large fibril bundles, perfect for characterization by cryo-EM. Solid-state NMR spectra showed only one set of resonances above the noise level at a signal-to-noise ratio of 10, thus suggesting that at least 90% of the A β monomers in the fibrils have the same fold^{8,14} without the need for further seeding. This suggests that the resulting fibril fold is the thermodynamically most stable structure at this pH value. In these "low-pH fibrils", the full N-terminus is part of the β -sheet core, and the fibrils' structure has been determined to high resolution by cryo-EM and solid-state NMR spectroscopy and has been described as an "LS-shape".8

The effect of a pH shift on amyloid fibrils was studied previously by Shammas and co-workers. 15 For insulin fibrils prepared at pH 2 and suspended in buffers with different pH values, they could show that the fibrils are highly stable at low pH values (pH 2.0-4.0). For pH values from 4.0 to 8.0, the disruption of specific electrostatic interactions leads to structural reorganization and a reduced β -strand network.¹ For the model system β_2 -micoglobulin (β_2 m), Tipping and coworkers reported that the stability of amyloid fibrils is highly pH-dependent and that even mild acidification enhances the formation of toxic fibril-derived oligomeric species. 16 The observation that amyloid fibrils, once formed, are not stable at every pH value could be shown in several other studies: amyloid fibrils formed by hormones are able to release monomers at pH 6 and pH 7.4.¹⁷ Additionally, the pHdependence of fibril disassembly of β -endorphin fibrils was investigated at pH 5.5 and pH 7.4 and found to be significantly faster at pH 5.5 compared to pH 7.4. 18 For PI3K-SH3 fibrils, it was observed that a pH change from 2 to 7.4 leads to almost complete decomposition of the fibrils after 1 h.¹⁹

For biophysical investigations such as interaction studies with physiological and diagnostic binding partners, reliable and reproducible (see Figure S1) in vitro generation of $A\beta(1-42)$ fibrils with a high degree of homogeneity and known structure is desirable. However, such studies should be conducted under physiological conditions, i.e., at pH values above 4. Thus, knowledge about the stability and structure of this fibril type at high pH values is essential for exploiting the high homogeneity of these well-characterized monomorphic LS fibrils, which are not obtained by fibrillization at higher pH values.

Here, we probe the stability and morphology of those lowpH A β (1-42) fibrils over the investigated pH range from 2 to 7. A change to higher pH values results in lateral association and bundling of amyloid filaments (vide infra, Figure 1A), thus preventing high-resolution structural analysis by cryo-EM. Solid-state NMR spectroscopy, on the other hand, probes the local environment of the nuclei and is, therefore, not affected by macroscopic rearrangements of filaments. Since solid-state NMR spectroscopy generally offers site-specific resolution, it can be used to probe the fibril structure as well as the protonation state of individual titratable groups. Further details were obtained from molecular dynamics (MD) simulations and complementary biophysical techniques, including AFM and CD spectroscopy and solution NMR spectroscopy.

RESULTS AND DISCUSSION

LS-Shaped A β (1–42) Fibrils Are Stable over the pH **Range 2 to 7.** A β (1–42) fibrils grown at acidic pH were adjusted to pH values ranging from 2.6 to 7.0 by adding a citrate-phosphate buffer to the fibril preparation. To test

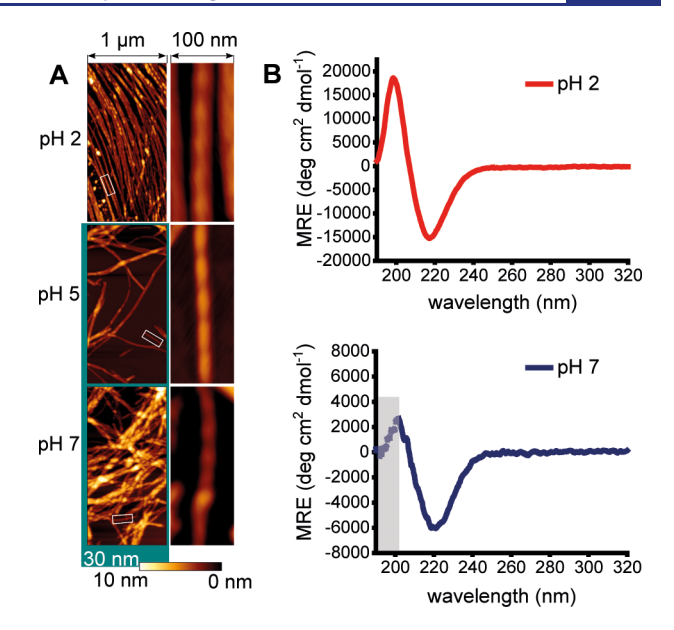


Figure 1. AFM images and CD spectra of $A\beta(1-42)$ fibrils at different pH values. (A) AFM images of $A\beta(1-42)$ fibrils under various pH conditions. Height profiles of the fibrils at original pH 2.0 and of fibrils shifted to pH 5.0 and 7.0 are shown: 1 μ m \times 2 μ m overview images (left column) and 100 nm × 250 nm single fibril cutouts (right column). The color scale from dark brown to white represents heights from 0 to 10 nm, or to 30 nm (highlighted in teal). Upon changing the pH from acidic toward neutral, the fibrils tend to form clusters instead of being present individually. Nevertheless, single fibrils are detectable also at neutral pH, exhibiting the characteristic periodicity. Its interval is in accordance with the 1160 \pm 199 Å helical pitch of A β (1–42) fibrils grown under equivalent acidic conditions.⁸ (B) CD (mean residue ellipticity (MRE)) spectra of A β (1–42) fibrils exhibit minima at 218 nm (pH 2.0) or 218–222 nm (pH 7.0) and x-axis intercepts at 207 nm (pH 2.0) or 208 nm (pH 7.0), characteristic for β -sheet dominated structures. At pH 7.0 extended fibril bundling and precipitation leads to a reduced S/N ratio, and below wavelengths of 200 nm (gray box) the number of photons reaching the detector is insufficient for reliable quantification. Likewise, the exact position of the minimum in the pH 7.0 spectrum may be affected by the rather high noise level.

whether the fibrils are preserved up to pH 7.0, we recorded AFM images of the samples at all pH values. The AFM images of these pH-shifted fibrils are shown in Figure 1A and Figure S2A. The addition of citrate-phosphate buffer resulted in increased clustering of the fibrils, in particular at pH 5.0, which is close to the isoelectric point of the peptide (5.3). This clustering also leads to signal reduction in the CD spectra (due to absorption flattening 20-22), which otherwise are highly similar and typical for a β -sheet-dominated structure (Figure 1B). However, the overall appearance, diameter, and periodicity of the fibrils, which are the signatures of a fibril polymorph, did not change, showing that the fibrils did not dissolve upon pH shift and that their morphology was generally preserved (Figure S2). A commonly used probe to detect amyloid fibril formation in vitro is the fluorescent dye thioflavin T (ThT). However, the ThT absorption and fluorescence emission intensity is highly pH-dependent,² and there are reports of a decrease in ThT fluorescence intensity at low pH values. 24,25 Indeed, A β fibrils grown in 30% acetonitrile (ACN), 0.1% TFA at pH 2.0 show no detectable ThT fluorescence increase (Figure S2B), but they are readily observable by AFM (Figure S2A). A pH variation between

pH 2.0 and 7.5 (at a constant ACN concentration of 24%) shows a strong pH dependence of ThT fluorescence intensity in the presence of A β fibrils with almost no fluorescence below pH 2.6 but increasing fluorescence with increasing pH (Figure S2B). Variation of the organic solvent content (between 1.5% and 24% ACN) at constant pH 2.0 or pH 7.0 in the presence of fibrils indicates that the ThT fluorescence is also highly ACN concentration-dependent (Figure S3B), with decreasing fluorescence at increasing ACN concentrations. Thus, our data indicate that ThT fluorescence alone is not suitable for detecting A β fibrils under the growth conditions applied (30% ACN, 0.1% TFA, pH 2).

Free ThT has been reported to undergo protonation of the dimethylamino group at low pH with a concomitant decrease in fluorescence intensity.²³ A pH titration of free ThT in citrate-phosphate buffer with 24% ACN monitored by NMR spectroscopy reveals that protonation is only detectable below pH 3.5 and remains negligibly small at pH 3.0 and pH 2.6 (Figure S4). Accordingly, the fluorescence intensity of ThT alone does not show any significant variation between pH 2.0 and 7.5 if the experimental uncertainties are taken into account (Figure S2B). We conclude that the lower sensitivity of the ThT assay at acidic pH cannot be explained by the properties of ThT alone without taking into account the interaction between ThT and A β fibrils. Consistent with the general notion that ThT primarily binds to grooves oriented parallel to the fibril axis, 26 MD simulations of ThT binding to LS-shaped $A\beta$ fibrils at pH 2.0 revealed that protonated ThT binds along the fibril axis at a surface-exposed groove formed by the side chains of V18, F20, and E22 on either protofilament with calculated affinities in the low micromolar range.²⁷ It is conceivable that the pH-induced electrostatic changes of the $A\beta$ fibrils, such as those described below, modulate ThT binding modes, affinities, and fluorescence properties in the bound state and that high ACN concentrations compete with ThT binding at this hydrophobic groove.

To test the effect of a pH shift on the fibril structure at the atomic level, we recorded $^{13}\mathrm{C}/^{13}\mathrm{C}$ and $^{15}\mathrm{N}/^{13}\mathrm{C}$ correlation solid-state NMR spectra on fibrils at different pH values. $^{13}\mathrm{C}$ chemical shifts of backbone and uncharged side chain atoms are mainly influenced by backbone and side chain torsion angles, whereas shifts of carboxyl groups are sensitive reporters on the protonation state. In fact, NMR spectroscopy is the only method that can determine protonation on a residue-specific level. The addition of citrate-phosphate buffer, which was used for adjusting the pH value, does not affect the overall $\mathrm{A}\beta(1{-}42)$ fibril structure, as evident from the comparison of 2D PDSD (proton-driven spin diffusion) $^{13}\mathrm{C}/^{13}\mathrm{C}$ correlation spectra of fibrils near pH 2 in the presence and absence of buffer (Figure S5).

The effect of a pH shift from 2 to 7 on the fibril structure can be estimated from an overlay of two PDSD spectra of fibrils at pH 2 (red) and pH 7 (blue) (Figure 2A, more details can be found in Figure S6). Most of the resonances observed at pH 2 and pH 7 coincide, indicating that most of the fold of the fibrils does not change when the pH is changed. Decreased intensities were observed for the N-terminus (residues D1 to G9), the His residues (H6, H13, H14), and K16. Figure 2D gives an estimate of relative intensities between selected cross peaks in two pairs of PDSD spectra (with short and long initial CP contact times of 100 and 1000 μ s) recorded on samples at pH 2 and pH 7, where the bulk $C\alpha/C\beta$ cross peak of the overlapping resonances of five Val residues was used for

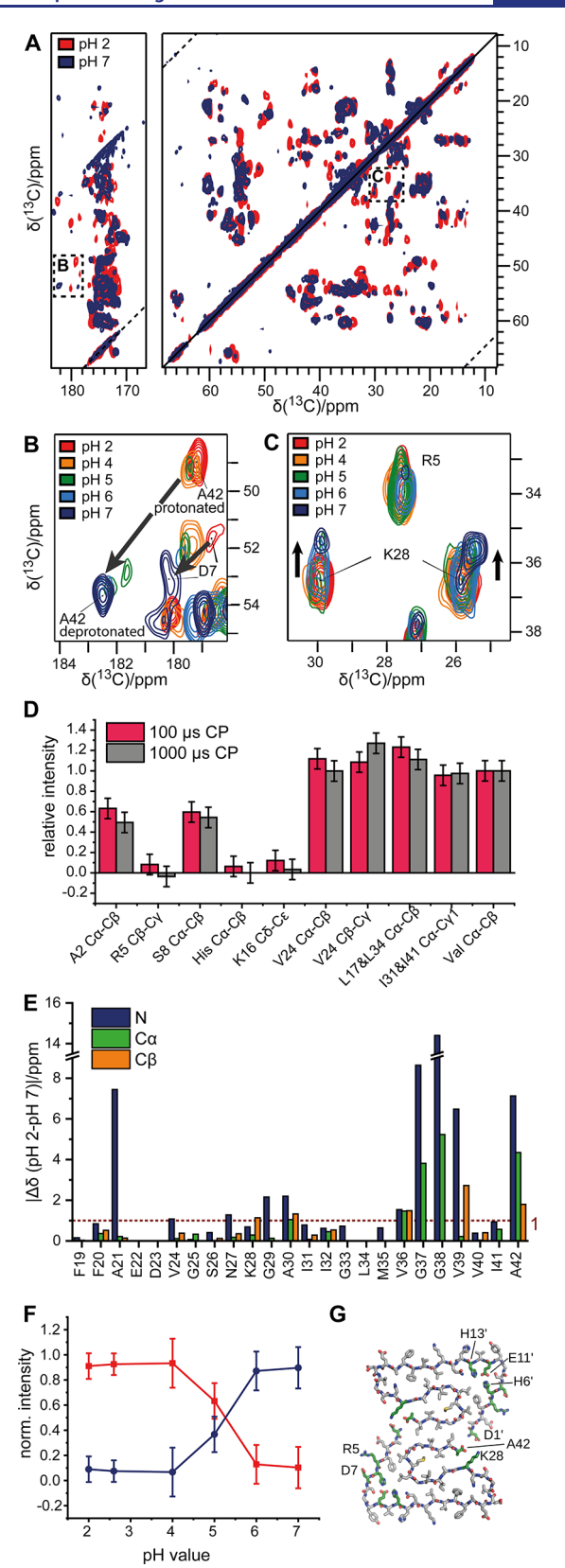


Figure 2. pH-induced local changes of $A\beta(1-42)$ fibrils as seen by solid-state NMR spectroscopy. (A) Overlay of 2D $^{13}C-^{13}C$ PDSD spectra of $A\beta(1-42)$ fibrils at pH 2 (red) and pH 7 (navy). For a more detailed view, see Figure S5. The chemical shift assignment for pH 2 was published in ref 8. As most of the signals are superimposing, the fold of the $A\beta(1-42)$ fibrils remains unchanged. (B, C) Zoomedin region from the overlay of the carboxyl (B) and the aliphatic (C)

Figure 2. continued

regions of the PDSD spectra at pH 2 (red), pH 4 (orange), pH 5 (green), pH 6 (blue), and pH 7 (navy). The pH shift influences especially the residues in the salt bridges (D1-K28 and adjacent A42, R5-D7). (D) Relative cross peak intensities of selected N- and Cterminal amino acid residues in PDSD spectra of the pH 7 fibril sample, normalized to the respective cross peaks in PDSD spectra recorded under identical conditions at pH 2. For each sample, two sets of PDSD spectra were recorded with initial ¹H-¹³C contact times of 100 μ s (red) and 1000 μ s (gray), respectively, and a mixing time of 20 ms. Spectra of the two samples were referenced to the bulk $C\alpha/C\beta$ cross peak of five Val residues (without V24), and the relative peak intensities for cross peak (i), $I_{\rm rel}^{(i)}$, were calculated as follows: $I_{\rm rel}^{(i)} = I({\rm pH7})^{(i)} \cdot I({\rm pH2})^{({\rm Val\ bulk})} / I({\rm pH2})^{(i)} \cdot I({\rm pH7})^{({\rm Val\ bulk})}$. (E) Chemical shift perturbation plot for pH 2 vs pH 7. (F) Normalized intensities for the A42 CO-C α correlation signals (in the protonated and deprotonated state) from the 2D CC are plotted against the pH value. The intensities were normalized using the following equations: $I_{\text{norm}}(\text{prot}) = (I(\text{prot})/(I(\text{prot}) + I(\text{deprot})) \text{ and } I_{\text{norm}}(\text{deprot}) = 1 - I(\text{deprot})$ I_{norm}(prot). The C-terminal A42 carboxyl group is completely protonated up to pH 4. For pH 5 and 6, both states can be observed, while the carboxyl group is to a high degree deprotonated at pH 7. Further details with chemical shifts from acidic amino acids and A42 can be found in Table S1. (G) The atomic model of the $A\beta(1-42)$ fibril (PDB: 50QV Gremer et al., 20178) shown as a stick model. Amino acids assumed essential for stabilizing the protofilament are colored in green. The structure with all labels is also shown in Figure S8). Spacing of contour levels in 2D spectra is 1.4 for (A) and 1.2 for (B) and (C).

normalization. $C\alpha/C\beta$ cross peak intensities of the well-resolved N-terminal residues A2 and S8 were reduced to ~50% of the intensity of corresponding cross peaks in spectra of pH 2 samples; $C\alpha/C\beta$ cross peaks of His residues, which may be affected by changes in side chain protonation, and side chain cross peaks of R5 and K16 are reduced to below 10% of the intensities of respective signals at pH 2. $C\alpha/C\beta$ correlations as well as side chain cross peaks of C-terminal residues are not reduced after the pH change. These findings are indicative of slightly increased dynamics for the backbone of the N-terminus and strongly enhanced mobility for the side chains of N-terminal residues at pH 7.

Despite intensity losses, the correlation signals of all Nterminal residues remain visible in the cross-polarization (CP)based ¹³C-spectra (Figure 2A, Figure S6), in contrast to $A\beta(1-$ 42) fibril structures having a flexible N-terminus.⁵⁻⁷ Intensity losses in CP spectra are an indication of enhanced mobility in the µs-ms regime. No protein resonance signals have been detected in Insensitive Nuclei Enhanced by Polarization Transfer (INEPT)³³ spectra at all pH values (Figure S7A,B), excluding isotropic motions in the sub- μ s regime, which would be indicative of highly dynamic or flexible parts or the presence of monomers in the sample. We also could not observe any additional protein signal in the direct excitation (DE) spectra compared to the CP spectra (Figure S7C). These findings suggest that the full $A\beta(1-42)$ peptide stays within the cross- β core of the fibril even at neutral pH. The L-shape of the Nterminal residues is destabilized with increased dynamics at

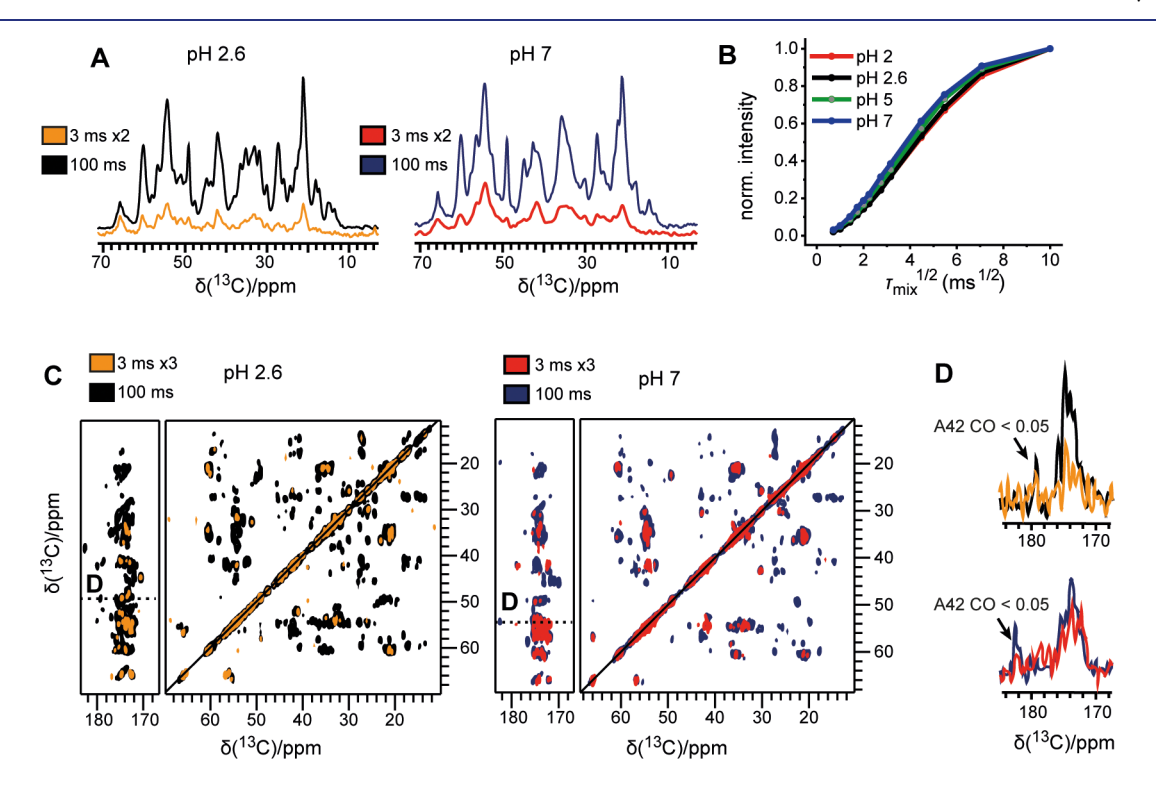


Figure 3. Water accessibility of $A\beta(1-42)$ fibrils at different pH conditions. (A) Aliphatic region of water-edited 1D ¹³C CP spectra at pH 2.6 and pH 7, measured with ¹H-¹H mixing times of 3 and 100 ms. Spectra recorded with short (3 ms) mixing time were recorded with twice the number of scans as those with long mixing time (100 ms). (B) pH-dependent water buildup curves for different pH values. A faster buildup with increasing pH values can be observed due to faster chemical exchange at increased pH values. (C) Water-edited 2D ¹³C-¹³C PDSD spectra of $A\beta(1-42)$ fibrils at pH 2.6 and pH 7 with a ¹H-¹H mixing time of 3 and 100 ms. In spectra recorded with a 3 ms mixing time, the number of scans was three times higher than for those recorded with long mixing time (100 ms). (D) 1D ¹³C cross sections taken from the A42 Cα chemical shifts at 49.3 ppm (pH 2.6) and 53.6 ppm (pH 7). A42 CO signals show low relative water-transferred intensities of less than 0.05. For the complete cross section of A42 and the cross section of the hydrophobic Ile side chains, see Figure S12. Spacing of contour levels in 2D spectra is 1.2.

pH 7, but some residual structure is retained, as indicated by weaker but unshifted CP signals.

For a more detailed insight, we also recorded 2D $^{15}N-^{13}C$ (NCaCX and NCOCX, Figure S8) spectra for pH 2 and pH 7. As the $A\beta(1-42)$ fibril preparation is reproducible, most resonances are the same for the pH 2 sample compared to previously published results. Most backbone residues could be *de novo* sequentially assigned for pH 7 starting from F19 (chemical shifts are deposited in the BMRB under the accession code 51584). As the NC transfer is a stronger mobility filter than a $^{13}C/^{13}C$ spin diffusion transfer, only the most rigid parts of the fibrils contribute to the $^{15}N/^{13}C$ correlation spectra. Thus, N-terminal residues up to V18 and the side chains of some residues are not visible in the NC spectra at pH 7 (Figure S8), whereas most signals can still be found in the PDSD spectrum.

In Figure 2E a chemical shift perturbation plot displaying chemical shift differences for $C\alpha$, $C\beta$, and N between pH 2 and pH 7 is shown. While chemical shifts for most 13 C atoms N-terminal of residue V36 do not change substantially (i.e., not more than 1.5 ppm for 13 C and 2.5 ppm for 15 N) with the pH value, we observe relatively large differences for the very C-terminal residues starting from G37 and especially for the two Gly residues G37 and G38. Furthermore, the 15 N shift of A21 is strongly affected by the pH shift, an effect that may be due to electrostatic interaction with the side chain of E22 that is deprotonated at pH 7. These changes are most likely caused by small conformational alterations in the C-terminus due to an alternative salt bridge formation (see next paragraph).

Deprotonation of Acidic Side Chains and Its Impact on the D1-K28 Salt Bridge. As expected from their pK_a values (intrinsic pKa values for Asp, Glu, and His as determined in blocked tri- or pentapeptides acetyl-Gly-X-Gly-amide or Ala-Ala-X-Ala-Ala are 3.9, 4.3, and 6.5, respectively^{32,34}), the protonation state of acidic amino acid residues is affected by a pH shift. This affects the stability of interresidual salt bridges, such as in the triad D1-K28-A42. Indeed, we observed shifts of several resonances for the carboxyl groups of D1, A42, D7, and the side chain resonances of K28 (Figure 2A and Figure S6). To observe at which pH value the changes start to occur, we performed a pH titration. In Figure 2B and Figure 2C, overlays of five spectra for fibrils between pH 2 and 7 are shown for two characteristic regions of the full spectrum. Up to pH 4, no changes were observed. Thus, we conclude that the overall protonation state of residues does not change up to this pH value. The effect of proton exchange at carboxyl and amino groups on the related NMR signals depends on the proton exchange rate relative to the frequency difference between the NMR resonances for the respective functional group in the protonated and the deprotonated state. 35,36 For fast proton exchange, we observe a progressive change in chemical shift, which reflects the population-weighted average between the protonated and deprotonated state (as observed for deprotonation of D7 (Figure 2B), a water-exposed residue at the fibril surface). For slow exchange by contrast, two resonances with populationdependent intensities are observed for the protonated as well as the deprotonated state (as seen for the C-terminal carboxyl group of A42 and for the side chain resonances of K28 (Figure $(2B,C)).^{3}$

In the $A\beta(1-42)$ fibril structure (Figure 2G, Figure S9), the interaction between protofilaments is stabilized by intermolecular salt bridges between D1 and K28 (Figure 4B).

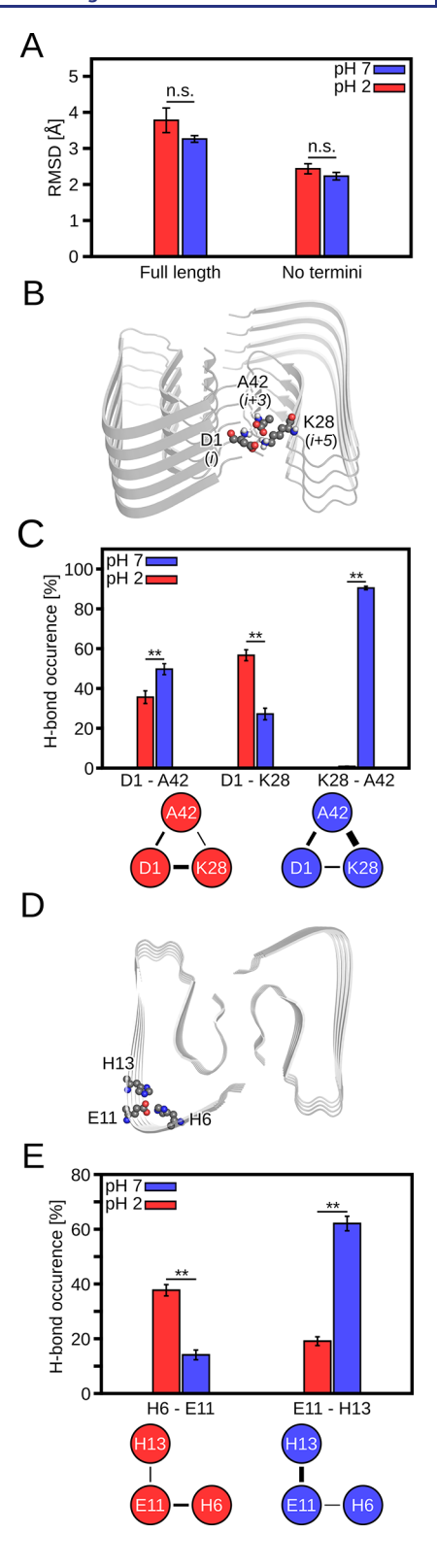


Figure 4. Interactions essential for fibril stability at acidic and neutral pH. (A) Mean backbone RMSD (n=10) for the full-length fibril and the fibril core in which the four terminal A β peptides were not considered during RMS fitting. (B) Fibril cryo-EM structure⁸ with amino acids crucial for inter-subunit stability depicted as spheres. (C) Average occurrence frequency of hydrogen bond interactions (from left to right n=17, n=15, and n=18) between amino acids shown in (B). The lower panel shows a schematic of the interactions, with black lines depicting the strength of interactions (scaled according to average occurrence). (D) Fibril cryo-EM structure⁸ with amino acids

Figure 4. continued

crucial for the stability of the N-terminal region depicted as spheres. (E) Average occurrence frequency of hydrogen bond interactions (n=20) between residues shown in (D). The lower panel shows a schematic of the interactions, with black lines depicting the strength of interactions (scaled according to average occurrence). In (A), (C), and (E), the error bars denote the standard error of the mean (SEM) (*p < 0.05; **p < 0.01; n.s. not significantly different).

Furthermore, the N-terminus is close to the C-terminal A42 of another $A\beta(1-42)$ monomer in the adjacent protofilament, which appears to be largely protonated at pH 2. A change to higher pH values has the following effects on the three residues involved in this triad interaction:

- The protonation/deprotonation of the terminal carboxyl group of A42 exhibits a slow exchange between two states (Figure 2B): The carboxyl group of A42 (intrinsic pK_a value for C-terminal Ala in a tripeptide: 3.55^{32}), protonated and β -strand-like at pH 2 and pH 4, adopts a deprotonated random coil-like conformation (with a CO shift of 182 ppm, in agreement with Wälti and Coworkers') at pH 6 and pH 7 (Table S1). Both states can be observed at pH 5 (with a splitting for the deprotonated random coil-like resonances, Figure 2B). These findings can also be observed for NCa spectra (Figure S10A). Fitting the peak intensities of NCa and PDSD peaks to the Henderson-Hasselbalch equation (Figure 2F and Figure S10B,C) leads to a pK_a value of 5.4 for C-terminal A42. The random-coil-like chemical shifts of deprotonated A42 are very similar to those obtained from solution NMR at pH 7 (Figure S11).
- Likewise, for K28 the pH shift to pH 7 induces a splitting of the K28 C β resonance typical for slow exchange (Figure 2C, Figure S6I). One resonance signal has the chemical shift of 35.6 ppm, as already observed at lower pH values, while a second signal is detected at a lower chemical shift of 35.3 ppm. Additional minor shifts occurred for K28 C ε resonances at pH 7. The signal splitting points toward the existence of a second alternative conformation of the K28 side chain. The relatively high Cy chemical shift of the amino acid residue D1 is indicative of a predominantly deprotonated state (\sim 90–95% deprotonation) already at pH 2. Comparing the D1 and D7 side chains at pH 2.0 and the slightly enhanced pH 2.6, we can already observe the following tendencies: D7 shows an increased degree of deprotonation with increasing pH values, whereas for D1, the degree of deprotonation seems to even slightly decrease with increasing pH values (Figure S5B). The detailed degree of deprotonation of all residues at pH 2 and pH 7 is shown in Table S1.

These observations can be explained as follows: At acidic pH values, the intermolecular salt bridge between the (almost) fully deprotonated D1 and the positively charged K28 stabilizes the fibril structure, whereas for the C-terminal carboxyl group the protonated state seems to be favored up to its p K_a of 5.4. In fact, a shift of the p K_a value by +1.9 pH units with respect to the intrinsic p K_a of 3.55 can easily be explained by the high density of negative charges³⁸ present in an amyloid fibril, and similar effects have already been described for fibrillary self-assembly of FMoc-diphenylalanine³⁹ and fibril

formation of α -synuclein. With increasing pH, the progressive deprotonation of A42 favors an additional interaction between the negatively charged C-terminal carboxyl group with K28, weakening the salt bridge between D1 and K28. This could explain the slightly enhanced protonation of D1 at pH 7 and the intensity losses for residues in the N-terminus at higher pH values, which are indicative of higher mobility. Matching our observations, MD simulations by Yin and co-workers indicated that the salt bridge between K28 and A42 leads to enhanced stability of the C-terminal deprotonated $A\beta(1-42)$ protofilaments compared to the protonated counterpart. The rearrangement of salt bridges in the triad between D1, K28, and A42 also influences the adjacent residues S26 (Figure S6D) and may also be responsible for conformational changes around the G37/G38 glycine pair (Figure 2E).

These findings are also supported by water-edited NMR spectroscopy, 42-44 where ¹H polarization transfer from water onto the protein is used to probe the water accessibility of amino acid residues on a residue-specific level (Figure 3, Figure S12): With an initial ¹H spin echo (duration 2.5 ms), transverse magnetization on the solid protein but not the mobile water molecules is dephased irreversibly by strong dipolar couplings. In a subsequent longitudinal mixing step (1 to 100 ms), ¹H polarization is transferred back to the protein and can then be detected in standard 1D or 2D solid-state NMR experiments (Figure S12A). As seen in Figure 3A and 3B, the overall magnetization transfer dynamics from water to the fibril is only slightly enhanced for pH 7 compared to pH 2. The small magnitude of this enhancement can be accounted for by faster chemical exchange at neutral pH, 45,46 while the relative fibril-water interface remains the same (as seen for the Ile residues, Figure S12B,C). For one Asp residue (D1, Figure S12D), however, the exchange with water is strongly accelerated at pH 7, indicating that the carboxyl group is more water-exposed, a finding that supports a weakened salt bridge. In contrast, A42 is still highly water protected at pH 7, as expected for the deprotonated carboxyl group of A42 forming a salt bridge to K28 (Figure 3D).

Monomers in Solution. Acetonitrile is not a routinely used cosolvent in protein NMR spectroscopy. To obtain a reliable reference for the solvent and pH effects on random coil chemical shifts and the conformational ensemble of monomeric A β (1–42), we also investigated [U–¹³C, ¹⁵N] A β (1–42) monomers in 28% acetonitrile at pH 2.0 (similar to the conditions used for fibril preparation), without acetonitrile at pH 2.0, and in citrate/phosphate buffer at pH 7.0 using solution NMR spectroscopy. Sequence-specific assignment of the 1H, 13C, and 15N backbone resonances of these three samples (BMRB access codes 51321, 51323, and 51322, respectively) reveals that $A\beta(1-42)$ monomers are highly disordered, with chemical shifts close to random coil values (Figure S11A) and low propensities for regular secondary structure elements under all these conditions. Accordingly, 2D $^{13}\text{C}-^{13}\text{C}$ total correlation (TOCSY) spectra of A β (1–42) monomers in 28% acetonitrile at pH 2.0 are very similar to those in Tris/HCl buffer at pH 7.2 (Figure S11B), except for the chemical shift changes expected due to different side chain protonation for Asp, Glu, and His residues. Thus, the influence of the pH on the fibril structure seems to be caused by the stabilization of the end product rather than any significant differences in monomer conformation.

MD Simulations for $A\beta(1-42)$ Fibrils with Different Protonation Degrees. We next performed MD simulations

of 1 μ s length of the A β (1–42) fibril with protonation states according to pH 2 and 7, with 10 replicas for each system (Figure S13) to provide a structural explanation at atomic resolution. The simulations revealed a shift in inter- and intramolecular polar interactions when going from pH 2 to pH 7, which preserves the structure and stability of the A β (1– 42) fibril.

Mean backbone root-mean-square differences (RMSD) < 4 Å indicate only minor structural changes among the differently protonated states, which are not significant (Figure 4A). Without the terminal $A\beta$ peptides, the mean RMSD decreases by ~1 Å (Figure 4A), indicating higher mobility of the terminal ${\rm A}\beta$ peptides, as corroborated by a peptide-wise RMSD analysis (Figure S14). Hence, the fibril core remains structurally stable at acidic and neutral pH, agreeing with our NMR experiments. However, as the fibril in our simulations is much smaller than in NMR experiments, our simulations likely overestimate the structural changes between fibrils of different protonation states.⁴⁷

Next, we investigated the changes in the fibril's interaction network between pH 2 and pH 7. The interactions among D1, K28, and the carboxyl group of A42 connect three A β peptides in the two protofilaments (Figure 4B). In line with our previous findings,8 changes in the protonation state of the Cterminus of A42 (Figure 4B) do not lead to a collapse of the fibril. Our MD simulations suggest that the interactions between D1, K28, and A42 are significantly different at pH 2 and pH 7 (Figure 4C). In particular, hydrogen bond interactions between the N-terminus of D1 and the Cterminus of A42 are significantly more frequent at pH 7 (Figure 4C). This can be explained by attractive forces between the oppositely charged N- and C-termini at pH 7. At pH 2, on the other hand, the A42 C-terminus is neutral after protonation, which reduces the likelihood for interactions with the still positively charged D1 N-terminus. On the other hand, the interaction between the side chain of D1 and K28 is reduced substantially at pH 7, but this loss is compensated by a strong interaction between A42 and K28 (Figure 4C). Overall, our MD simulations suggest that interactions involving D1, K28, and A42 occur in the fibril at pH 7. At pH 2, however, when the C-terminus of A42 is protonated, D1 and K28 likely form salt bridges between the protofilaments, which agrees with the results obtained by cryo-EM.8 That way, interactions between protofilaments are formed in an A42-independent manner.

At pH 2, the L-shaped N-terminus is stabilized by salt bridges between the positively charged H6 and H13 and the negatively charged E118 (Figure 4D). These interactions are present at pH 2 and 7 but with a different frequency of occurrence. At pH 2, E11 preferentially interacts with H6 (Figure 4E). As H6 is harbored on the small leg of the Lshaped N-terminus (Figure 4D), this interaction is likely essential for stabilizing the whole N-terminal region. At pH 7, E11 preferentially interacts with H13 on the large β -strand, which may weakly destabilize the N-terminus (Figure 4E).

To conclude, our simulations revealed a rebalancing of intrasubunit (H6/E11/H13) and inter-subunit (D1/K28/A42) interactions between fibrils with protonation states at pH 2 and pH 7, providing a plausible explanation of why most of the structure of the LS-shaped fibril grown at pH 2 remains unchanged between the two pH conditions.

CONCLUSION

In summary, we showed that the structure of the $A\beta(1-42)$ fibril remains unchanged when grown at acidic pH and adjusted to neutral pH values afterward. However, upon pH adjustment, changes in the amino acid protonation states are observed for the residues A42, D1, and K28 as well as for E11 and H6/H13, as summarized in Figure 5. Although intra-

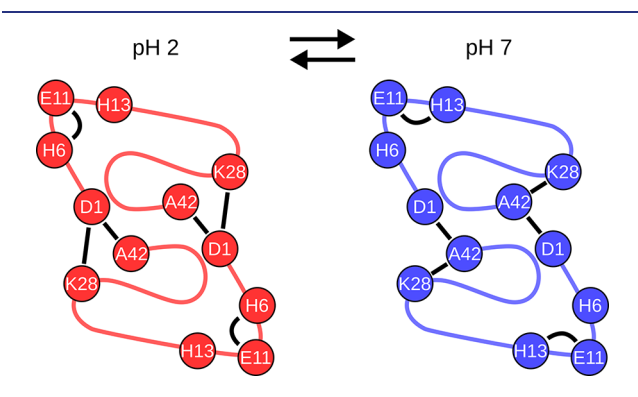


Figure 5. Model of interactions essential for fibril stability at acidic and neutral pH. Schematic of the $A\beta(1-42)$ fibril investigated in the present study (pH conditions shown above). Amino acids identified to be essential for structural stability are depicted by circles and oneletter amino acid codes. Interactions between amino acids are shown as black bars. The $A\beta(1-42)$ backbone is traced by a line.

subunit and inter-subunit salt bridges are rearranged as a consequence of deprotonation, fibrils remained stable up to pH 7. Performing a pH titration, we excluded any changes until pH 4 but observed a few specific changes in protonation at pH 6 and more pronounced at pH 7, with protonation states being populated at pH 2 at the respective sites. Our study strongly suggests that the A β (1–42) fibril grown at acidic pH⁸ conserves its structure and remains stable at physiological pH conditions. Thus, $A\beta(1-42)$ fibrils grown at pH 2 can be used over the full pH range from pH 2 to pH 7 for binding and interaction studies.

ASSOCIATED CONTENT

Supporting Information

The Supporting Information is available free of charge at https://pubs.acs.org/doi/10.1021/jacs.2c09231.

Additional experimental details, materials and methods, and additional results (AFM, CD, ThT fluorescence intensities, NMR spectra, and chemical shifts) (PDF)

Accession Codes

Sequence-specific assignment of the ¹H, ¹³C, and ¹⁵N backbone resonances of $A\beta(1-42)$ monomers in 28% ACN at pH 2.0, without ACN at pH 2.0, and in citrate/phosphate buffer at pH 7.0 using solution NMR spectroscopy are deposited in the Biological Magnetic Resonance Data Bank (BMRB) under the access codes 51321, 51323, and 51322, respectively. Sequencespecific solid-state NMR resonance assignments of ¹⁵N and ¹³C resonances of A β (1–42) fibrils shifted to pH 7.0 are deposited in the BMRB under the access code 51584.

AUTHOR INFORMATION

Corresponding Authors

Henrike Heise — Institute of Biological Information Processing (IBI-7: Structural Biochemistry) and JuStruct: Jülich Center

for Structural Biology, Forschungszentrum Jülich, 52425 Jülich, Germany; Physikalische Biologie, Heinrich-Heine-Universität Düsseldorf, 40225 Düsseldorf, Germany; orcid.org/0000-0002-9081-3894; Email: henrike.heise@uni-duesseldorf.de

Holger Gohlke — Institute of Biological Information Processing (IBI-7: Structural Biochemistry) and JuStruct: Jülich Center for Structural Biology, Forschungszentrum Jülich, 52425 Jülich, Germany; John von Neumann Institute for Computing (NIC), Jülich Supercomputing Centre (JSC), Forschungszentrum Jülich GmbH, 52425 Jülich, Germany; Institute for Pharmaceutical and Medicinal Chemistry, Heinrich Heine University Düsseldorf, 40225 Düsseldorf, Germany; orcid.org/0000-0001-8613-1447; Email: gohlke@uni-duesseldorf.de

Authors

Nina Becker — Institute of Biological Information Processing (IBI-7: Structural Biochemistry) and JuStruct: Jülich Center for Structural Biology, Forschungszentrum Jülich, 52425 Jülich, Germany; Physikalische Biologie, Heinrich-Heine-Universität Düsseldorf, 40225 Düsseldorf, Germany; orcid.org/0000-0002-6617-2775

Benedikt Frieg — Institute of Biological Information Processing (IBI-7: Structural Biochemistry) and JuStruct: Jülich Center for Structural Biology, Forschungszentrum Jülich, 52425 Jülich, Germany; John von Neumann Institute for Computing (NIC), Jülich Supercomputing Centre (JSC), Forschungszentrum Jülich GmbH, 52425 Jülich, Germany; orcid.org/0000-0002-7877-0262

Lothar Gremer — Institute of Biological Information Processing (IBI-7: Structural Biochemistry) and JuStruct: Jülich Center for Structural Biology, Forschungszentrum Jülich, 52425 Jülich, Germany; Physikalische Biologie, Heinrich-Heine-Universität Düsseldorf, 40225 Düsseldorf, Germany; orcid.org/0000-0001-7065-5027

Tatsiana Kupreichyk — Institute of Biological Information Processing (IBI-7: Structural Biochemistry) and JuStruct: Jülich Center for Structural Biology, Forschungszentrum Jülich, 52425 Jülich, Germany; Physikalische Biologie, Heinrich-Heine-Universität Düsseldorf, 40225 Düsseldorf, Germany; orcid.org/0000-0002-5151-6424

Luis Gardon — Institute of Biological Information Processing (IBI-7: Structural Biochemistry) and JuStruct: Jülich Center for Structural Biology, Forschungszentrum Jülich, 52425 Jülich, Germany; Physikalische Biologie, Heinrich-Heine-Universität Düsseldorf, 40225 Düsseldorf, Germany; orcid.org/0000-0003-0871-6487

Patrick Freiburg – Physikalische Biologie, Heinrich-Heine-Universität Düsseldorf, 40225 Düsseldorf, Germany

Philipp Neudecker — Institute of Biological Information Processing (IBI-7: Structural Biochemistry) and JuStruct: Jülich Center for Structural Biology, Forschungszentrum Jülich, 52425 Jülich, Germany; Physikalische Biologie, Heinrich-Heine-Universität Düsseldorf, 40225 Düsseldorf, Germany; orcid.org/0000-0002-0557-966X

Dieter Willbold — Institute of Biological Information Processing (IBI-7: Structural Biochemistry) and JuStruct: Jülich Center for Structural Biology, Forschungszentrum Jülich, 52425 Jülich, Germany; Physikalische Biologie, Heinrich-Heine-Universität Düsseldorf, 40225 Düsseldorf, Germany; orcid.org/0000-0002-0065-7366

Complete contact information is available at:

https://pubs.acs.org/10.1021/jacs.2c09231

Author Contributions

N.B., B.F., and L.G. contributed equally to this work. **Notes**

The authors declare no competing financial interest.

ACKNOWLEDGMENTS

We acknowledge experimental assistance by Dr. Ü. Akbey and Dr. D. Schölzel, access to the Jülich-Düsseldorf Biomolecular NMR Center jointly run by Forschungszentrum Jülich and Heinrich Heine University Düsseldorf (HHU), computational support and infrastructure provided by the "Zentrum für Informations- und Medientechnologie" at HHU, and computing time provided by the John von Neumann Institute for Computing (NIC) to H.G. and B.F. on the supercomputer JUWELS at Jülich Supercomputing Centre (JSC) (user IDs: HKF7, VSK33). This work was supported by the Deutsche Forschungsgemeinschaft (DFG) (HE 3243/4-1, INST 208/771-1 FUGG, and INST 208/620-1 FUGG).

REFERENCES

- (1) Selkoe, D. J.; Hardy, J. The amyloid hypothesis of Alzheimer's disease at 25 years. *EMBO molecular medicine* **2016**, 8 (6), 595–608. (2) Vassar, R.; Bennett, B. D.; Babu-Khan, S.; Kahn, S.; Mendiaz, E. A.; Denis, P.; Teplow, D. B.; Ross, S.; Amarante, P.; Loeloff, R.; Luo, Y.; Fisher, S.; Fuller, J.; Edenson, S.; Lile, J.; Jarosinski, M. A.; Biere, A. L.; Curran, E.; Burgess, T.; Louis, J.-C.; Collins, F.; Treanor, J.; Rogers, G.; Citron, M. β -Secretase Cleavage of Alzheimer's Amyloid Precursor Protein by the Transmembrane Aspartic Protease BACE. *Science* **1999**, 286 (5440), 735–741.
- (3) Chiti, F.; Stefani, M.; Taddei, N.; Ramponi, G.; Dobson, C. M. Rationalization of the effects of mutations on peptide and protein aggregation rates. *Nature* **2003**, 424 (6950), 805–8.
- (4) Meisl, G.; Yang, X.; Hellstrand, E.; Frohm, B.; Kirkegaard, J. B.; Cohen, S. I.; Dobson, C. M.; Linse, S.; Knowles, T. P. Differences in nucleation behavior underlie the contrasting aggregation kinetics of the $A\beta$ 40 and $A\beta$ 42 peptides. *Proc. Nat. Acad. Sci. U.S.A.* **2014**, *111* (26), 9384–9.
- (5) Xiao, Y.; Ma, B.; McElheny, D.; Parthasarathy, S.; Long, F.; Hoshi, M.; Nussinov, R.; Ishii, Y. $A\beta(1-42)$ fibril structure illuminates self-recognition and replication of amyloid in Alzheimer's disease. *Nat. Struct. Mol. Biol.* **2015**, 22, 499.
- (6) Colvin, M. T.; Silvers, R.; Ni, Q. Z.; Can, T. V.; Sergeyev, I.; Rosay, M.; Donovan, K. J.; Michael, B.; Wall, J.; Linse, S.; Griffin, R. G. Atomic Resolution Structure of Monomorphic $A\beta$ 42 Amyloid Fibrils. J. Am. Chem. Soc. **2016**, 138 (30), 9663–9674.
- (7) Wälti, M. A.; Ravotti, F.; Arai, H.; Glabe, C. G.; Wall, J. S.; Böckmann, A.; Güntert, P.; Meier, B. H.; Riek, R. Atomic-resolution structure of a disease-relevant $A\beta(1-42)$ amyloid fibril. *Proc. Natl. Acad. Sci. U. S. A.* **2016**, *113* (34), E4976–E4984.
- (8) Gremer, L.; Schölzel, D.; Schenk, C.; Reinartz, E.; Labahn, J.; Ravelli, R. B. G.; Tusche, M.; Lopez-Iglesias, C.; Hoyer, W.; Heise, H.; Willbold, D.; Schröder, G. F. Fibril structure of amyloid- β (1–42) by cryo-electron microscopy. *Science* **2017**, 358 (6359), 116–119.
- (9) Yang, Y.; Arseni, D.; Zhang, W.; Huang, M.; Lövestam, S.; Schweighauser, M.; Kotecha, A.; Murzin, A. G.; Peak-Chew, S. Y.; Macdonald, J.; Lavenir, I.; Garringer, H. J.; Gelpi, E.; Newell, K. L.; Kovacs, G. G.; Vidal, R.; Ghetti, B.; Ryskeldi-Falcon, B.; Scheres, S. H. W.; Goedert, M. Cryo-EM structures of amyloid- β 42 filaments from human brains. *Science* 2022, 375 (6577), 167–172.
- (10) Qiang, W.; Yau, W. M.; Lu, J. X.; Collinge, J.; Tycko, R. Structural variation in amyloid- β fibrils from Alzheimer's disease clinical subtypes. *Nature* **2017**, *541* (7636), 217–221.
- (11) Ghosh, U.; Yau, W.-M.; Collinge, J.; Tycko, R. Structural differences in amyloid- β fibrils from brains of nondemented elderly

- individuals and Alzheimer's disease patients. Proc. Nat. Acad. Sci. U. S. A. 2021, 118 (45), No. e2111863118.
- (12) Wickramasinghe, A.; Xiao, Y.; Kobayashi, N.; Wang, S.; Scherpelz, K. P.; Yamazaki, T.; Meredith, S. C.; Ishii, Y. Sensitivity-Enhanced Solid-State NMR Detection of Structural Differences and Unique Polymorphs in Pico- to Nanomolar Amounts of Brain-Derived and Synthetic 42-Residue Amyloid- β Fibrils. *J. Am. Chem. Soc.* **2021**, *143* (30), 11462–11472.
- (13) Schütz, A. K.; Vagt, T.; Huber, M.; Ovchinnikova, O. Y.; Cadalbert, R.; Wall, J.; Güntert, P.; Böckmann, A.; Glockshuber, R.; Meier, B. H. Atomic-Resolution Three-Dimensional Structure of Amyloid β Fibrils Bearing the Osaka Mutation. *Angew. Chem., Int. Ed.* **2015**, *54* (1), 331–335.
- (14) Willbold, D.; Strodel, B.; Schröder, G. F.; Hoyer, W.; Heise, H. Amyloid-type Protein Aggregation and Prion-like Properties of Amyloids. *Chem. Rev.* **2021**, *121* (13), 8285–8307.
- (15) Shammas, S. L.; Knowles, T. P. J.; Baldwin, A. J.; MacPhee, C. E.; Welland, M. E.; Dobson, C. M.; Devlin, G. L. Perturbation of the Stability of Amyloid Fibrils through Alteration of Electrostatic Interactions. *Biophys. J.* **2011**, *100* (11), 2783–2791.
- (16) Tipping, K. W.; Karamanos, T. K.; Jakhria, T.; Iadanza, M. G.; Goodchild, S. C.; Tuma, R.; Ranson, N. A.; Hewitt, E. W.; Radford, S. E. pH-induced molecular shedding drives the formation of amyloid fibril-derived oligomers. *Proc. Natl. Acad. Sci. U. S. A.* **2015**, *112* (18), 5691–5696.
- (17) Maji, S. K.; Perrin, M. H.; Sawaya, M. R.; Jessberger, S.; Vadodaria, K.; Rissman, R. A.; Singru, P. S.; Nilsson, K. P. R.; Simon, R.; Schubert, D.; Eisenberg, D.; Rivier, J.; Sawchenko, P.; Vale, W.; Riek, R. Functional Amyloids As Natural Storage of Peptide Hormones in Pituitary Secretory Granules. *Science* **2009**, 325 (5938), 328–332.
- (18) Nespovitaya, N.; Gath, J.; Barylyuk, K.; Seuring, C.; Meier, B. H.; Riek, R. Dynamic Assembly and Disassembly of Functional β -Endorphin Amyloid Fibrils. *J. Am. Chem. Soc.* **2016**, *138* (3), 846–856.
- (19) Röder, C.; Vettore, N.; Mangels, L. N.; Gremer, L.; Ravelli, R. B. G.; Willbold, D.; Hoyer, W.; Buell, A. K.; Schröder, G. F. Atomic structure of PI3-kinase SH3 amyloid fibrils by cryo-electron microscopy. *Nat. Commun.* **2019**, *10* (1), 3754.
- (20) Duysens, L. N. The flattening of the absorption spectrum of suspensions, as compared to that of solutions. *Biochim. Biophys. Acta* **1956**, *19* (1), 1–12.
- (21) Gordon, D. J.; Holzwarth, G. Artifacts in the measured optic activity of membrane suspensions. *Arch. Biochem. Biophys.* **1971**, *142* (2), 481–8.
- (22) Miles, A. J.; Wallace, B. A. Circular dichroism spectroscopy of membrane proteins. *Chem. Soc. Rev.* **2016**, *45* (18), 4859–4872.
- (23) Hackl, E. V.; Darkwah, J.; Smith, G.; Ermolina, I. Effect of acidic and basic pH on Thioflavin T absorbance and fluorescence. *Eur. Biophys. J.* **2015**, 44 (4), 249–261.
- (24) LeVine, H. Thioflavine T interaction with amyloid β -sheet structures. *Amyloid* **1995**, 2 (1), 1–6.
- (25) Groenning, M.; Norrman, M.; Flink, J. M.; van de Weert, M.; Bukrinsky, J. T.; Schluckebier, G.; Frokjaer, S. Binding mode of Thioflavin T in insulin amyloid fibrils. *J. Struct Biol.* **2007**, *159* (3), 483–97.
- (26) Krebs, M. R. H.; Bromley, E. H. C.; Donald, A. M. The binding of thioflavin-T to amyloid fibrils: localisation and implications. *J. Struct. Biol.* **2005**, *149* (1), 30–37.
- (27) Frieg, B.; Gremer, L.; Heise, H.; Willbold, D.; Gohlke, H. Binding modes of thioflavin T and Congo red to the fibril structure of amyloid- β (1–42). *Chem. Commun.* **2020**, *56* (55), 7589–7592.
- (28) Spera, S.; Bax, A. Empirical correlation between protein backbone conformation and C_{α} and $C_{\beta}^{13}C$ nuclear magnetic resonance chemical shifts. *J. Am. Chem. Soc.* **1991**, *113* (14), 5490–5492.
- (29) Wishart, D. S.; Case, D. A. Use of chemical shifts in macromolecular structure determination. *Nuclear Magnetic Resonance of Biological Macromolecules, Pt A* **2002**, 338, 3–34.

- (30) Oldfield, E. Chemical shifts in amino acids, peptides, and proteins: From quantum chemistry to drug design. *Annu. Rev. Phys. Chem.* **2002**, 53, 349–378.
- (31) Berjanskii, M. V.; Wishart, D. S. Unraveling the meaning of chemical shifts in protein NMR. *Biochimica et Biophysica Acta (BBA) Proteins and Proteomics* **2017**, *1865* (11), 1564–1576.
- (32) Platzer, G.; Okon, M.; McIntosh, L. P. pH-dependent random coil 1H, 13C, and 15N chemical shifts of the ionizable amino acids: a guide for protein pK $_{\rm a}$ measurements. *J. Biomol. NMR* **2014**, *60* (2), 109–129.
- (33) Andronesi, O. C.; Becker, S.; Seidel, K.; Heise, H.; Young, H. S.; Baldus, M. Determination of Membrane Protein Structure and Dynamics by Magic-Angle-Spinning Solid-State NMR Spectroscopy. *J. Am. Chem. Soc.* **2005**, *127* (37), 12965–12974.
- (34) Grimsley, G. R.; Scholtz, J. M.; Pace, C. N. A summary of the measured pK values of the ionizable groups in folded proteins. *Protein Sci.* **2008**, *18* (1), 247–251.
- (35) Keim, P.; Vigna, R. A.; Morrow, J. S.; Marshall, R. C.; Gurd, F. R. N. Carbon 13 Nuclear Magnetic Resonance of Pentapeptides of Glycine Containing Central Residues of Serine, Threonine, Aspartic and Glutamic Acids, Asparagine, and Glutamine. *J. Biol. Chem.* 1973, 248 (22), 7811–7818.
- (36) van der Cruijsen, E. A.; Prokofyev, A. V.; Pongs, O.; Baldus, M. Probing Conformational Changes during the Gating Cycle of a Potassium Channel in Lipid Bilayers. *Biophys. J.* **2017**, *112* (1), 99–108
- (37) Waudby, C. A.; Ramos, A.; Cabrita, L. D.; Christodoulou, J. Two-Dimensional NMR Lineshape Analysis. *Sci. Rep.* **2016**, *6* (1), 24826.
- (38) Jeppesen, M. D.; Westh, P.; Otzen, D. E. The role of protonation in protein fibrillation. *FEBS Lett.* **2010**, 584 (4), 780–784.
- (39) Tang, C.; Smith, A. M.; Collins, R. F.; Ulijn, R. V.; Saiani, A. Fmoc-Diphenylalanine Self-Assembly Mechanism Induces Apparent pK_a Shifts. *Langmuir* **2009**, 25 (16), 9447–9453.
- (40) Pálmadóttir, T.; Malmendal, A.; Leiding, T.; Lund, M.; Linse, S. Charge Regulation during Amyloid Formation of α -Synuclein. *J. Am. Chem. Soc.* **2021**, 143 (20), 7777–7791.
- (41) Yin, X.; Liu, S.; Perez-Aguilar, J. M.; Zhou, H.; Shao, Q.; Yang, Z.; Zhou, R. Different protonated states at the C-terminal of the amyloid-beta peptide modulate the stability of S-shaped protofibril. *J. Chem. Phys.* **2019**, *150* (18), 185102.
- (42) Lesage, A.; Böckmann, A. Water-Protein Interactions in Microcrystalline Crh Measured by 1H-13C Solid-State NMR Spectroscopy. J. Am. Chem. Soc. 2003, 125 (44), 13336–13337.
- (43) Ader, C.; Schneider, R.; Seidel, K.; Etzkorn, M.; Becker, S.; Baldus, M. Structural Rearrangements of Membrane Proteins Probed by Water-Edited Solid-State NMR Spectroscopy. *J. Am. Chem. Soc.* **2009**, *131* (1), 170–176.
- (44) Williams, J. K.; Hong, M. Probing membrane protein structure using water polarization transfer solid-state NMR. *J. Magn. Reson.* **2014**, 247, 118–127.
- (45) Mandala, V. S.; Loftis, A. R.; Shcherbakov, A. A.; Pentelute, B. L.; Hong, M. Atomic structures of closed and open influenza B M2 proton channel reveal the conduction mechanism. *Nat. Struct. Mol. Biol.* **2020**, *27* (2), 160–167.
- (46) Gelenter, M. D.; Mandala, V. S.; Niesen, M. J. M.; Sharon, D. A.; Dregni, A. J.; Willard, A. P.; Hong, M. Water orientation and dynamics in the closed and open influenza B virus M2 proton channels. *Commun. Biol.* **2021**, *4* (1), 338.
- (47) König, C.; Skånberg, R.; Hotz, I.; Ynnerman, A.; Norman, P.; Linares, M. Binding sites for luminescent amyloid biomarkers from non-biased molecular dynamics simulations. *Chem. Commun.* **2018**, 54 (24), 3030–3033.